Asociación Argentina
de Mecánica Computacional

Mecánica Computacional Vol XXXIX, págs. 901-910 (artículo completo)
F.E. Dotti, M. Febbo, S.P. Machado, M. Saravia, M.A. Storti (Eds.)
Bahía Blanca, 1-4 Noviembre 2022

ANALYSIS OF FLOW PULSE PROPAGATION IN ELASTIC PIPES FOR THE ESTIMATION OF ARTERIAL STIFFNESS

Sofía S. Sarraf[a], Ezequiel J. López[a], Jorge D'Elía[b] and Damián Craiem[c]

[a]*Instituto de Investigación en Tecnologías y Ciencias de la Ingeniería, Universidad Nacional del Comahue-CONICET, Buenos Aires 1400, 8300 Neuquén, Argentina*
sofia.sarraf@fain.uncoma.edu.ar, ezequiel.lopez@fain.uncoma.edu.ar

[b]*Centro de Investigación en Métodos Computacionales, Universidad Nacional del Litoral-CONICET, Predio CONICET "Dr. Alberto Cassano", Colectora RN 168 s/n – Paraje El Pozo, 3000 Santa Fe, Argentina*
jdelia@cimec.unl.edu.ar

[c]*Instituto de Medicina Traslacional, Transplante y Bioingeniería, Universidad Favaloro-CONICET, Solis 453, 1078 Ciudad Autónoma de Buenos Aires, Argentina*
dcraiem@favaloro.edu.ar

Keywords: Flow pulse, Pulse Wave Velocity, Blood flow, Fluid-Structure Interaction.

Abstract. Pulse Wave Velocity (PWV) in arteries is a valuable marker for the determination of the vessel stiffness, as it correlates with geometrical and biomechanical parameters of the artery wall. In addition, the PWV can be obtained non-invasively using Cardiac Magnetic Resonance Imaging. For straight vessels of constant diameter and thickness, the PWV is given by the Moens-Korteweg (M-K) equation, which indicates a direct proportionality between the square of the PWV and the elastic modulus of the wall material, its thickness and the inverse of the vessel diameter. In this work we performed three-dimensional simulations of flow pulses in straight elastic pipes and we compare the results with the M-K equation estimations. It was assumed that the flow is incompressible and the pipe wall has a linear elastic behaviour. A suitable absorbing boundary condition was designed in order to avoid wave reflections at the outflow border. The coupling between the fluid and structure solvers was carried out by a Dirichlet-to-Neumann strategy using the IQN-ILS (Interface Quasi-Newton with Inverse Jacobian from Least-Squares) method. The fluid transport properties and the mechanical properties of the pipe wall had physiologically realistic values similar to those found in the abdominal aorta, as well as the geometrical dimensions of the pipe. The PWV was computed as the distance between two transversal planes divided by the transit time for a given pressure (or flow rate) amplitude level in both planes. Several configurations were analyzed, including variations in the elastic modulus of the wall tissue, wall thickness and initial pipe diameter. The results obtained for the PWV are in good agreement with the M-K prediction.

1 INTRODUCTION

Cardiovascular diseases are one of the main causes of death worldwide and the early evaluation of arterial stiffness has shown to improve risk prevention (Arnett et al., 2019). The left ventricular ejection produces pulsatile pressure and flow waves that propagate from the heart and through the aorta to the rest of arterial tree and the body. Since the aorta is the main conduit artery of the systemic circuit, that also cushions the waves pulsatility, the assessment of aortic pulse wave velocity (PWV) as a surrogate of arterial stiffness could bring valuable information (Milan et al., 2019). PWV can be non-invasively estimated using tonometry as the ratio between the distance of two simultaneous pressure measurements and propagation waves transit time (TT) (Davies and Struthers, 2003). Besides ultrasound, recent advances in cardiac magnetic resonance allow a precise assessment of aortic geometry in the three dimensions and blood flow at distinct transversal planes to have a better insight of regional aortic stiffness (Jarvis et al., 2022). During pathological aortic dilatations, such observed in bicuspid patients, medical treatments are mostly decided based on the vessel size whereas estimations of stiffness biomarkers are still under debate (Pascaner et al., 2021). A detailed knowledge and understanding of the transmission mechanisms of pressure and flow waves using CFD (Computational Fluid Dynamics) with FSI (Fluid-Structure Interaction) in idealized tubular models can help to improve these diagnostic methods. CFD analyses have been successfully employed to study the hemodynamic impact of aortic aneurysms before and after endovascular treatments (Dottori et al., 2020). In simple straight vessels of constant diameter and thickness, the PWV can be analytically estimated using the Moens-Korteweg (M-K) equation, which indicates a direct proportionality between the square root of the PWV and the wall elastic modulus, its thickness and the inverse of the vessel diameter (Shahmirzadi et al., 2012). The main assumptions of the M-K equation include an infinite straight and cylindrical tube with elastic, isotropic and homogeneous walls, incompressible and non-viscous fluid. Under these idealized conditions, special attention should be paid to reducing the effects of reflected waves such as to minimize errors in TT calculations (Segers et al., 2009).

In this work we performed three-dimensional (3D) simulations of flow pulses in straight elastic pipes that modeled the abdominal aorta and we compare the results with the M-K equation estimations.

2 MATHEMATICAL MODELS

The blood flow is modeled as incompressible, isothermal and with Newtonian behaviour. In order to account for the fluid domain deformation the ALE (Arbitrary Lagrangian-Eulerian) formulation is applied. The governing equations for this flow are the continuity

$$\nabla \cdot \mathbf{u} = 0 \quad \text{in } \Omega_f \times [t_0,\, t_f] \tag{1}$$

and the linear momentum conservation law:

$$\frac{\partial \mathbf{u}}{\partial t} + [(\mathbf{u} - \mathbf{w}) \cdot \nabla]\mathbf{u} = -\frac{1}{\rho_f}\nabla p + \frac{\mu}{\rho_f}\nabla \cdot (\nabla \mathbf{u} + \nabla^T \mathbf{u}) \quad \text{in } \Omega_f \times [t_0,\, t_f] \tag{2}$$

where t is the time, $\mathbf{u}$ is the flow velocity, p is the pressure, ρ_f is the fluid density, μ is the dynamic viscosity of the fluid, $\mathbf{w}$ is the moving coordinate velocity in the ALE formulation, Ω_f is the fluid domain, and $[t_0,\, t_f]$ is the time interval.

The vessel wall is assumed as a linear elastic solid governed by the following equation

$$\rho_s \frac{\partial^2 \mathbf{v}}{\partial t^2} = \nabla \cdot \boldsymbol{\sigma}_s \quad \text{in } \Omega_s \times [t_0,\, t_f] \tag{3}$$

where $\mathbf{v}$ is the displacement of the solid, ρ_s is the solid density, and $\boldsymbol{\sigma}_s$ is the strain tensor given by the standard Hooke's law

$$\boldsymbol{\sigma}_s = \frac{E}{1+\nu}\left[\nabla\mathbf{v} + (\nabla\mathbf{v})^T + \frac{\nu}{1-2\nu}\text{tr}(\nabla\mathbf{v})\mathbf{I}\right] \tag{4}$$

E being the Young modulus, ν the Poisson coefficient, and $\mathbf{I}$ the second order tensor identity. No external forces are considered. In Eq. (3) the symbol Ω_s represents the solid domain.

On the fluid-solid interface Γ_i the following conditions must be fulfilled:

- Kinematical conditions: continuity of the displacement and velocity on Γ_i, *i.e.*

$$\begin{aligned} \mathbf{v}_f &= \mathbf{v}_s \\ \mathbf{u}_f &= \mathbf{u}_s \end{aligned} \tag{5}$$

  where subscripts f and s refer to the fluid and the solid, respectively.

- Dynamic condition: equilibrium of forces on Γ_i

$$\mathbf{n}\cdot\boldsymbol{\sigma}_f = \mathbf{n}\cdot\boldsymbol{\sigma}_s \tag{6}$$

  where $\mathbf{n}$ is the unit vector normal to Γ_i and $\boldsymbol{\sigma}_f = \mu(\nabla\mathbf{u} + \nabla^T\mathbf{u}) - p\mathbf{I}$.

3 NUMERICAL SCHEME AND SOLUTION ALGORITHM

The mathematical problem previously presented is numerically solved using the FVM (Finite Volume Method) on a collocated grid. In particular, the `solids4Foam` toolbox (Cardiff et al., 2018) is used and compiled with `foam-extend-4.1`.

A partitioned strategy is applied to solve the equation system (1)-(3), where each equation is solved one at a time in an iterative process. The governing equations for the fluid are solved in this work using the PISO (Pressure-Implicit with Splitting of Operators, Issa (1986)) algorithm. The equations for the solid are solved splitting the surface force term into implicit and explicit components, and solving for each component of the unknown vector in a segregated way. For more details, see Cardiff et al. (2018) and the references therein.

3.1 Fluid-structure coupling

As previously said, the fluid and solid problems are solved using a partitioned approach. Then, a coupling method must be applied in order to enforce conditions (5) and (6) on the interface. The Dirichlet-to-Neumann coupling methodology is used in the present work, where the fluid is solved imposing velocities at the interface (Dirichlet condition) whereas the solid is solved imposing tractions at the interface (Neumann condition).

To improve the coupling convergence, the IQN-ILS (Interface-Quasi-Newton with Inverse Jacobian from Least-Squares, Degroote et al. (2009)) method is used. The IQN-ILS method is a matrix-free algorithm which is based on approximating the increment of the fluid-solid interface unknowns (the product of minus the residual by the inverse of the jacobian matrix) as linear combinations of the residuals previously computed. This linear combination is updated as iterations proceeds. The coefficients of the linear combination are calculated solving an over-determined system applying a least-squares method (Degroote et al., 2009). It was shown that the IQN-ILS performs equally or better than other interface coupling methods (Degroote et al., 2010).

3.2 Outlet boundary condition

The set of governing equations (1)-(2) and (3) have a hyperbolic behaviour when applied to an elastic tube modeled as a one-dimensional domain, which is a widely used model for simulating large arteries (Anliker et al., 1971; Olufsen, 1999). If the tube is modeled in 3D, as in the present work, wave-like solutions are also expected. Nevertheless, since the solution algorithm is partitioned, in each iteration the fluid is computed as incompressible. This means, for instance, that a velocity or pressure perturbation at inlet triggers a perturbation at outlet in the first iterations of the coupling algorithm. Of course, as iterations proceed the algorithm corrects the solution and, if convergence is reached, the perturbation travels at finite speed.

In any case, boundary conditions must be imposed at the outlet section for both, pressure and velocity. A typical boundary condition used at outflows for incompressible flows is to impose a given value for pressure. However, for the kind of problem considered here this choice will produce the reflection of waves at the outlet. Therefore, an absorbing boundary condition must be applied at the outflow in order to avoid wave reflection.

The one-dimensional model of the problem has two characteristic directions with characteristic velocities $\lambda^{\pm} = u \pm c$ (Anliker et al., 1971), where u is the axial velocity (z direction in this work) and c is the local wave speed given by

$$c = \sqrt{\frac{S}{\rho_f (\partial S/\partial p)_z}} \tag{7}$$

S being the cross-sectional area of the pipe.

The M-K equation can be derived from Eq. (7) assuming circular pipe with radius r and wall thickness h, $h/r << 1$, axial-symmetry in the problem, and supposing that the change in the cross-sectional is negligible (William, 1982). Under these hypothesis the M-K equation is obtained and given by

$$c = \sqrt{\frac{Eh}{2\rho_f r}} \tag{8}$$

Following with the one-dimensional model and assuming that the tube is initially straight, that there are no inflow/outflow across the wall and neglecting the viscous friction, the compatibility equations are given by (Anliker et al., 1971)

$$du \pm \frac{dp}{\rho_f c} = 0 \tag{9}$$

For a simple wave traveling in the $(+)$ direction (from left to right in the axial direction), the characteristic variable representing wave components in the $(-)$ direction are null everywhere in the domain. Then, in that case the following relation holds:

$$u - \frac{p}{\rho_f c} = 0 \tag{10}$$

The outlet boundary condition applied in this work is based on the expression (10). For a simple wave traveling from left to right and an outlet section being the rightmost cross-section of the pipe, the condition imposed for pressure reads

$$p = \rho_f c(\mathbf{u} \cdot \mathbf{n}) \tag{11}$$

where $\mathbf{n}$ is the outward unit normal to the outflow section and c is assumed constant and approximated with the M-K equation (8). Due to the simplifications and approximations involved in deriving Eq. (11), this condition is not perfectly absorbing and it is called in this work a quasi-absorbing condition.

4 METHODS

In this work, models and methods presented in sections §2 and §3 will be applied to simulate blood flow pulses through arteries in order to estimate the PWV. To this end, a fragment of an artery was modeled as an initially straight cylinder with internal radius r, wall thickness h and axial length L (see Fig. 1). A base case was defined as reference, for which $r = 15$ mm, $h = 1.5$ mm, $L = 500$ mm, $E = 0.407$ MPa and $\nu = 0.3$. The remaining properties of the fluid and solid were kept constant with the following values: $\rho_s = 1000$ kg/m^3, $\rho_f = 1060$ kg/m^3, and $\mu = 4 \times 10^{-3}$ Pa s. From the base case, six additional cases were solved considering variations of ± 10 % in r, h and E, one at a time.

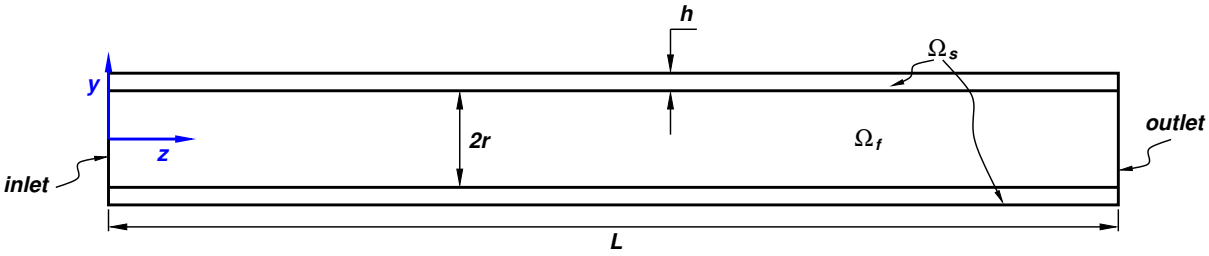

Figure 1: Sketch of the mid-plane of the problem domain.

At the fluid inlet, a time-varying velocity approximating a physiological measured flow rate in an aorta was imposed (flow volume of 35.8 ml per heartbeat). Figure 2 shows the resulting flow rate profile for the base case. At that boundary zero normal gradient was imposed for pressure. At the outlet section, pressure was computed applying the quasi-absorbing boundary condition described in section §3.2 and zero normal gradient was imposed for velocity. The cylinder wall was fixed at both ends and zero traction was imposed on its external boundary. For the initial condition, the fluid was at rest, the pressure was set to zero and the solid undeformed.

The fluid mesh has 125000 cells with 250 equidistant cells along the axial direction and grading towards the pipe wall. The solid mesh also has 250 equally-spaced cells in the axial direction and 3 cells in the wall thickness, totalizing 30000 cells. The mesh dynamics of the fluid was solved applying the Laplacian technique for the mesh velocity using a diffusion coefficient proportional to the inverse distance to the pipe wall. The final simulation time was 1 s, corresponding to one heartbeat according to the available data, and the time step used in all cases was 0.001 s.

The PWV was computed using the TT of the pulse wave between two successive cross-sectional planes dividing the distance among them by the TT. The pulse signal was obtained from the 3D solution integrating the flow variables in each cross-section. The ascending part of the pulse was considered in order to define values of pressure or flow rate for the TT calculation. These threshold values were adopted as percentages of the pulse maximum (peak). The corresponding TT was identified with the percentage as subscript. For instance, Fig. 2 shows the TT for the 50 % of maximum flow rate between two different cross-sectional planes. Transit times for a given value of pressure or flow rate were computed for adjacent cross-sectional planes, which were separated by 10 mm in the analysis presented in the following section and

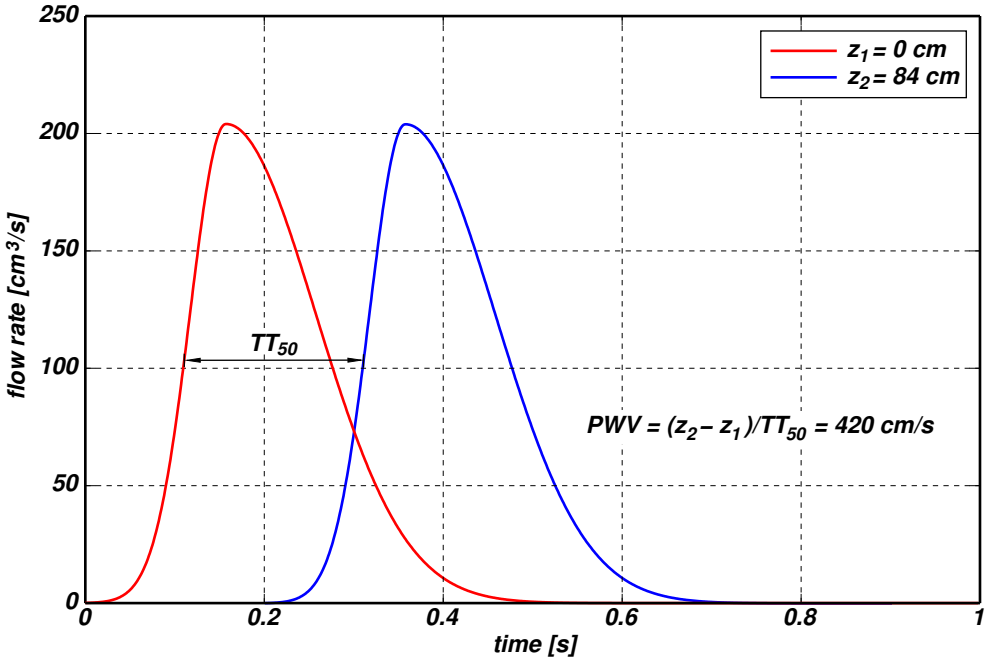

Figure 2: Flow rate profile imposed at inlet in the base case and definition of TT.

then represented in the $z - t$ plane. Finally, these points were approximated by a linear fitting and the PWV was estimated as the slope of that line.

5 RESULTS

As an example of the computed solutions, Fig. 3 shows the pressure field in the fluid (left) and the magnitude of the pipe wall displacement (right) for the base case at $t = 0.2$ s. At this time instant the peak of the pressure wave is located at $z = 170$ mm from the inlet, while the maximum displacement of the solid wall is below 1 mm.

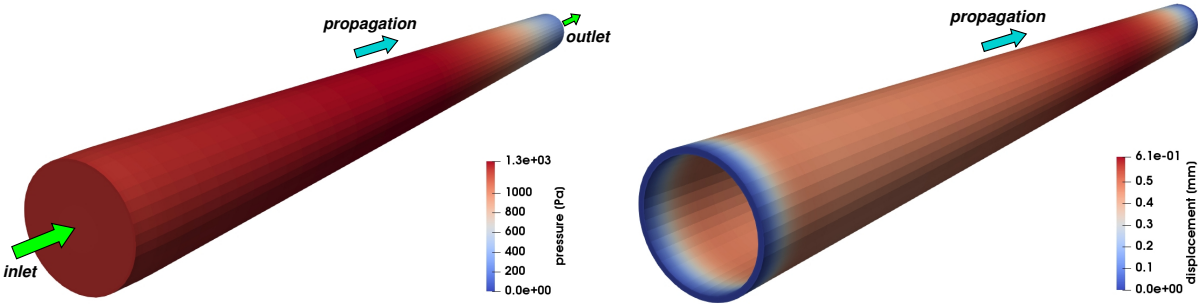

Figure 3: Solution at $t = 0.2$ s for the base case $r = 15$ mm, $h = 1.5$ mm, and $E = 0.407$ MPa. Left: pressure field in the fluid. Right: magnitude of displacement of the solid wall.

For the base case, Fig. 4 presents space-time developments of the flow rate and mean axial pressure. The TT_{50} (50% threshold) of the flow rate wave for cross-sectional planes distant 10 mm from each other are shown as red dots together with its linear fitting (Fig. 4, left). The slope of this line is 4.4052 m/s, which differs from the theoretical value of M-K (4.3816 m/s) in 0.54 %. Analogous data are shown for the pressure wave in Fig. 4 (right), using in this case the TT_{90} (90% threshold) and resulting a slope of the fitting line of 4.3303 m/s (difference of 1.17 % with respect to the M-K value).

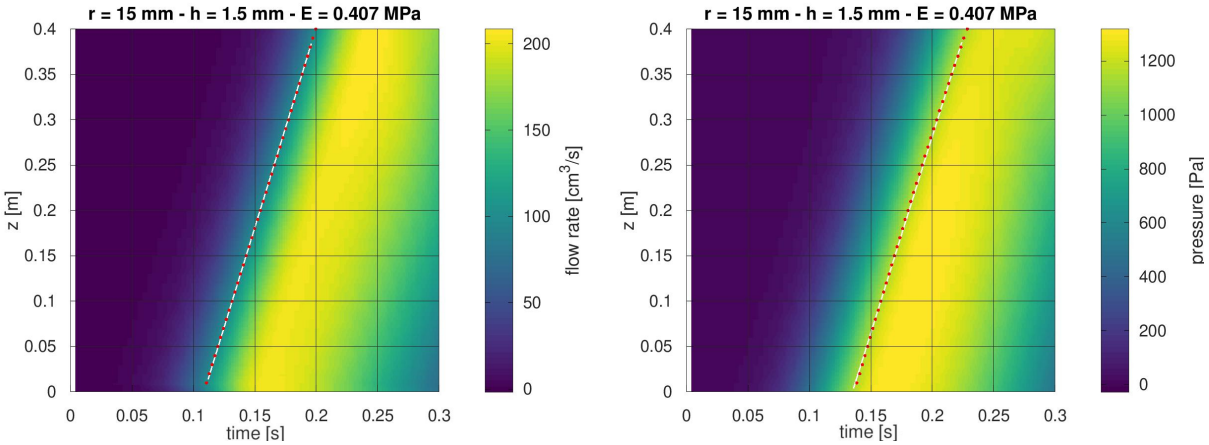

Figure 4: Space-time maps of flow rate (left) and mean axial pressure (right) for the base case. Red dots represent TT_{50} for the flow rate and TT_{90} for the pressure wave at different locations, linearly fitted with the white line.

Tables 1 and 2 present the results obtained extending the previous analysis to the remaining cases varying r, h and E. In general, the numerical results capture qualitative and quantitatively well the expected variations in the PWV due to modifications in the parameters affecting it. The percentage differences with respect to the M-K value are below 2 % except for the case with $r = 13.5$ mm, which reaches differences below 4 % using the flow rate wave and below 3 % using the pressure wave.

r [mm]	h [mm]	E [MPa]	M-K [m/s]	PWV [m/s]	Dif. [%]
15.0	1.50	0.4070	4.3816	4.4052	0.54
15.0	1.50	0.4477	4.5954	4.5257	1.52
15.0	1.50	0.3663	4.1567	4.1790	0.54
15.0	1.65	0.4070	4.5954	4.5038	1.99
15.0	1.35	0.4070	4.1567	4.1991	1.02
16.5	1.50	0.4070	4.1777	4.2240	1.11
13.5	1.50	0.4070	4.6186	4.4531	3.58

Table 1: PWV and porcentual difference with respect the M-K value obtained for the 7 simulated cases using the flow rate wave and TT_{50} (transit-time using 50 % threshold).

r [mm]	h [mm]	E [MPa]	M-K [m/s]	PWV [m/s]	Dif. [%]
15.0	1.50	0.4070	4.3816	4.3303	1.17
15.0	1.50	0.4477	4.5954	4.6577	1.36
15.0	1.50	0.3663	4.1567	4.1313	0.61
15.0	1.65	0.4070	4.5954	4.6468	1.12
15.0	1.35	0.4070	4.1567	4.1426	0.34
16.5	1.50	0.4070	4.1777	4.1738	0.09
13.5	1.50	0.4070	4.6186	4.7428	2.69

Table 2: PWV and porcentual difference with respect the M-K value obtained for the 7 simulated cases using the pressure wave and TT_{90} (transit-time using 90 % threshold).

6 DISCUSSION

In this study, the propagation of pulsatile pressure and flow waveforms through compliant cylindrical tubes has been simulated to assess a PWV as a surrogate for a vessel stiffness. Using the M-K equation as a theoretical reference, the simulation confirmed that an increase in the tube wall thickness or the elastic modulus proportionally increased the PWV squared and the relationship with radius was inverse. The application of CFD and dynamic FSI might now be extended to evaluate vessel stiffness under more complex arterial geometries.

In most cases, differences between theoretical PWV values and simulation measurements remained below 2%. These differences were relatively small considering that the variation of the parameters proposed in our study was around $\pm 10\%$, much smaller than in other reports where detectable variations ranged from -50% to +100% (Shahmirzadi et al., 2012). Increased differences were observed when the tube was shrank 10% and are supposed to be due to a higher ratio S/S_0, where S_0 is the initial cross-sectional area of the pipe. Although the theoretical value given by the M-K equation is used to compare the results of the simulation, it must be pointed out that this comparison is only a reference, since the goal was not to simulate cases under the hypothesis assumed in the M-K analysis.

The absorbing boundary condition adopted in our simulation at the tube outlet was effective to minimize backward wave reflections and helped to accurately assess the transit times.The estimation of PWV is based on the assessment of the TT between two pressure or flow waves at two locations separated by a known distance. The clinical method to estimate TT differs if signals are based on pressure or flow acquisitions. To avoid invasive pressure measurements using a catheter, non-invasive tonometric techniques are clinically employed (Davies and Struthers, 2003). The tonometric technique is based on placing a pressure sensor on the skin over superficial arteries (carotid-femoral or carotid-radial) and recording the signals simultaneously or synchronized by ECG (Electrocardiogram). The main limitations of this method are the estimation of an accurate distance between the two distinct sites and the fact that the biomarker represent regional and not local stiffness values. The assessment of 4D-Flow MRI (Magnetic Resonance Imaging) acquisitions are currently tested because they allow for a simultaneous assessment of blood flow curves at 2 distinct locations together with the exact 3D distance between the sites through the vessel centerline (Jarvis et al., 2022). Usually, the onset of the pressure or flow waves is used to determine TT but other methods including cross-correlation, maximum derivative or the peak time were also reported (Dogui et al., 2011). Backward wave reflections could interfere with the wave peak or even with the wave up-slope and also a physiological wave widening along the vessel path is usually expected (Grotenhuis et al., 2009). Accordingly, a 50% threshold was set in our study to determine TT using flow rate waves and a 90% threshold using pressure waves. Probably, pressure waves were less prone to noise around the wave peak. This decision was mostly justified as a good compromise thinking in our 4D-Flow MRI applications (Pascaner et al., 2021), where small velocities are noisy to accurately determine the foot of the flow wave and peak flow time might be contaminated by strong wave reflections. Further simulations in patient specific configurations should be investigated to choose the best TT measurement method, particularly in cases where a dilatation is observed such in patients with aortic aneurysms.

Some limitations of this work should be mentioned. The model assumed linear elastic walls when vessel elasticity is mostly non-linear. The idealized model could be somehow justified by the small observed deformations but more complex non-linear elastic models might also be evaluated in future numerical simulations. The geometry of a straight pipe was adopted to

match the conditions of the M-K equations. Even if some aortic regions, such as the thoracic descending or abdominal regions are mostly cylindrical, arterial morphology and flow patterns are extremely complex and particular locations like the the aortic arch include several bifurcations where our simplified model might not be valid. Moreover, arteries dilate and collapse, producing geometrical changes associated with variations in PWV that could interfere with the M-K stiffness association (Pascaner et al., 2021). Further simulations could be improved building 3D meshes from patient specific models based on computed tomography images.

7 CONCLUSION

Three-dimensional simulations of pressure/flow pulses propagation through elastic tubes with arterial dimensions were performed to evaluate PWV as an indirect marker of the tube stiffness. The most important parameters affecting the PWV were varied in the simulations, including the tube radius, the wall thickness and the Young modulus, obtaining the correct tendencies in the PWV values relative to the M-K equation with percent differences below 4 %. Based on these results we gained confidence on the methods and solvers applied in the present work, allowing its use in cases with more complex geometries such as those including regional variations in the radius, in the wall thickness, and/or patient-specific configurations.

ACKNOWLEDGMENTS

This work has received financial support from Consejo Nacional de Investigaciones Científicas y Técnicas (CONICET, Argentina), Universidad Nacional del Comahue (UNCo, Argentina, grant PIN 04/I-251), Universidad Nacional del Litoral (UNL, Argentina, grant CAI+D 2020 50620190100110LI), and Agencia Nacional de Promoción Científica y Tecnológica (ANPCyT, Argentina, grants PICT 2018-2920 and PICT 2019-1563), and was partially performed with the Free Software Foundation GNU-Project resources as GNU/Linux OS, GCC compilers, GNU/Octave, and GNUPlot, as well as other Open Source resources as OpenFOAM®, ParaView, and LaTeX, among many others.

REFERENCES

Anliker M., Rockwell R., and Oden E. Nonlinear analysis of flow pulses and shock waves in arteries. Part I: Derivation and properties of mathematical model. *Journal of Applied Mathematics and Physics (ZAMP)*, 22:217–246, 1971.

Arnett D.K., Blumenthal R.S., Albert M.A., Buroker A.B., Goldberger Z.D., Hahn E.J., Himmelfarb C.D., Khera A., Lloyd-Jones D., McEvoy J.W., et al. 2019 ACC/AHA guideline on the primary prevention of cardiovascular disease: a report of the American College of Cardiology/American Heart Association Task Force on Clinical Practice Guidelines. *Circulation*, 140(11):e596–e646, 2019.

Cardiff P., Karač A., De Jaeger P., Jasak H., Nagy J., Ivanković A., and Tuković Z. An open-source finite volume toolbox for solid mechanics and fluid-solid interaction simulations. 2018. doi:10.48550/ARXIV.1808.10736.

Davies J.I. and Struthers A.D. Pulse wave analysis and pulse wave velocity: a critical review of their strengths and weaknesses. *Journal of hypertension*, 21(3):463–472, 2003.

Degroote J., Bathe K.J., and Vierendeels J. Performance of a new partitioned procedure versus a monolithic procedure in fluid–structure interaction. *Computers and Structures*, 87(11-12):793–801, 2009.

Degroote J., Haelterman R., Annerel S., Bruggeman P., and Vierendeels J. Performance of

partitioned procedures in fluid–structure interaction. *Computers and Structures*, 88(7-8):446–457, 2010.

Dogui A., Redheuil A., Lefort M., DeCesare A., Kachenoura N., Herment A., and Mousseaux E. Measurement of aortic arch pulse wave velocity in cardiovascular MR: comparison of transit time estimators and description of a new approach. *Journal of Magnetic Resonance Imaging*, 33(6):1321–1329, 2011.

Dottori J., Casciaro M., Craiem D., El-Batti S., Mousseaux E., Alsac J.M., and Larrabide I. Regional assessment of vascular morphology and hemodynamics: methodology and evaluation for abdominal aortic aneurysms after endovascular repair. *Computer Methods in Biomechanics and Biomedical Engineering*, 23(14):1060–1070, 2020.

Grotenhuis H.B., Westenberg J.J., Steendijk P., van der Geest R.J., Ottenkamp J., Bax J.J., Jukema J.W., and de Roos A. Validation and reproducibility of aortic pulse wave velocity as assessed with velocity-encoded MRI. *Journal of Magnetic Resonance Imaging: An Official Journal of the International Society for Magnetic Resonance in Medicine*, 30(3):521–526, 2009.

Issa R. Solution of the implicitly discretised fluid flow equations by operator-splitting. *Journal of Computational Physics*, 62(1):40–65, 1986.

Jarvis K., Scott M.B., Soulat G., Elbaz M.S., Barker A.J., Carr J.C., Markl M., and Ragin A. Aortic pulse wave velocity evaluated by 4D flow MRI across the adult lifespan. *Journal of Magnetic Resonance Imaging*, 2022.

Milan A., Zocaro G., Leone D., Tosello F., Buraioli I., Schiavone D., and Veglio F. Current assessment of pulse wave velocity: comprehensive review of validation studies. *Journal of hypertension*, 37(8):1547–1557, 2019.

Olufsen M. Structured tree outflow condition for blood flow in larger systemic arteries. *American Journal of Physiology*, 276(1):257–268, 1999.

Pascaner A.F., Houriez S., Craiem D., Gencer U., Casciaro M.E., Charpentier E., Bouaou K., De Cesare A., Dietenbeck T., Chenoune Y., et al. Comprehensive assessment of local and regional aortic stiffness in patients with tricuspid or bicuspid aortic valve aortopathy using magnetic resonance imaging. *International Journal of Cardiology*, 326:206–212, 2021.

Segers P., Kips J., Trachet B., Swillens A., Vermeersch S., Mahieu D., Rietzschel E., De Buyzere M., and Van Bortel L. Limitations and pitfalls of non-invasive measurement of arterial pressure wave reflections and pulse wave velocity. *Artery research*, 3(2):79–88, 2009.

Shahmirzadi D., Li R.X., and Konofagou E.E. Pulse-wave propagation in straight-geometry vessels for stiffness estimation: theory, simulations, phantoms and in vitro findings. *Journal of biomechanical engineering*, 134(11), 2012.

William R. *Hemodynamics*. Williams & Wilkins, 1982. ISBN 978-0683060508.